Environmental Science & Technology

Article

Cite This: Environ. Sci. Technol. 2018, 52, 11699−11707

pubs.acs.org/est

Sensing Ocean Plastics with an Airborne Hyperspectral Shortwave Infrared Imager

Shungudzemwoyo P. Garaba,*[,†,‡,§] Jen Aitken,[†,∥] Boyan Slat,[†] Heidi M. Dierssen,[‡] Laurent Lebreton,[†,⊥] Oliver Zielinski,[§] and Julia Reisser[†,#,∇]

[†]The Ocean Cleanup Foundation, Batavierenstraat 15, Rotterdam 3014 JH, Netherlands

[‡]Department of Marine Sciences, Avery Point Campus, University of Connecticut, 1080 Shennecossett Road, Groton, Connecticut 06340, United States

[§]Marine Sensor Systems Group, Institute for Chemistry and Biology of the Marine Environment, Carl von Ossietzky University of Oldenburg, Schleusenstraße 1, Wilhelmshaven 26382, Germany

[∥]Teledyne Optech Inc., 7225 Stennis Airport Road #300, Kiln, Mississippi 39556, United States

[⊥]The Modelling House, 3 Bay View Road, Raglan 3225, New Zealand

[#]Australian Institute of Marine Science, Indian Ocean Marine Research Centre, 39 Fairway, Perth 6009, Australia

[∇]Red Sea Research Center, King Abdullah University of Science and Technology, Thuwal 23955, Saudi Arabia

ABSTRACT: Here, we present a proof-of-concept on remote sensing of ocean plastics using airborne shortwave infrared (SWIR) imagery. We captured red, green, and blue (RGB) and hyperspectral SWIR imagery with equipment mounted on a C-130 aircraft surveying the "Great Pacific Garbage Patch" at a height of 400 m and a speed of 140 knots. We recorded the position, size, color, and type (container, float, ghost net, rope, and unknown) of every plastic piece identified in the RGB mosaics. We then selected the top 30 largest items within each of our plastic type categories (0.6−6.8 m in length) to investigate SWIR spectral information obtained with a SASI-600 imager (950−2450 nm). Our analyses revealed unique SWIR spectral features common to plastics. The SWIR spectra obtained (N = 118 items) were quite similar both in magnitude and shape. Nonetheless, some spectral variability was observed, likely influenced by differences in the object optical properties, the level of water submersion, and an intervening atmosphere. Our simulations confirmed that the ∼1215 and ∼1732 nm absorption features have potential applications in detecting ocean plastics from spectral information. We explored the potential of SWIR remote sensing technology for detecting and quantifying ocean plastics, thus provide relevant information to those developing better monitoring solutions for ocean plastic pollution.

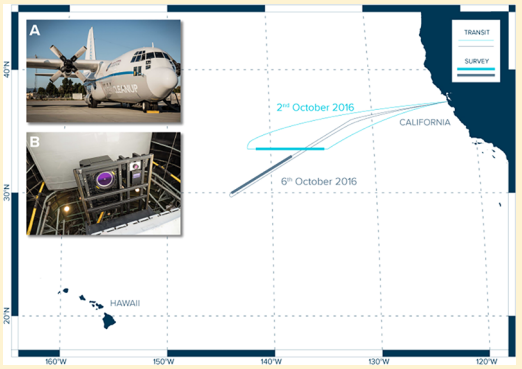

INTRODUCTION

As the amount of plastics in the natural environment escalates, there is an urgent need for technological, legislative, and policy solutions based on accurate scientific evidence-based research.[1,2] Unfortunately, a knowledge gap exists in terms of the temporal and spatial distribution of ocean plastics. Currently, there are only regional assessments of plastics on beaches, water columns, and the sea floor, for example, Arctic deep-sea sediments.[3] For buoyant ocean plastics, most of our knowledge is based on robust numerical modeling[4−6] coupled with limited data sets containing information on observed amounts of millimeter-sized plastics.[7,8] Buoyant ocean plastic pieces (or mass) per unit of sea surface area are commonly estimated using the number (or mass) of particles collected by small surface net tows, normalized by the surface area covered during the tows.[8−10] Although this technique has been extensively used and is a key source of information, it is very constrained both spatially and temporally. The models calibrated by these limited data sets provide estimated ocean plastic abundances, with geographical details of plastic pollution hotspots, including regions where plastics are entering the oceans, for example, estuarine systems and coastal populations,[9,11,12] as well as wide areas where plastics are accumulating, for example, subtropical oceanic gyres.[4−6,8,11,13] However, these numerical models only paint a rough picture of the ocean plastic distribution, mostly due to a lack of input data from field observations.

Buoyant ocean plastics seem to concentrate in the upper layer of oceans, mostly within the first 0.5 m.[14] As such, ocean plastic remote sensing from space and airborne platforms has the potential to be a reliable source of quantitative and

Received: May 28, 2018
Revised: August 15, 2018
Accepted: August 20, 2018
Published: September 25, 2018

DOI: 10.1021/acs.est.8b02855
Environ. Sci. Technol. 2018, 52, 11699−11707

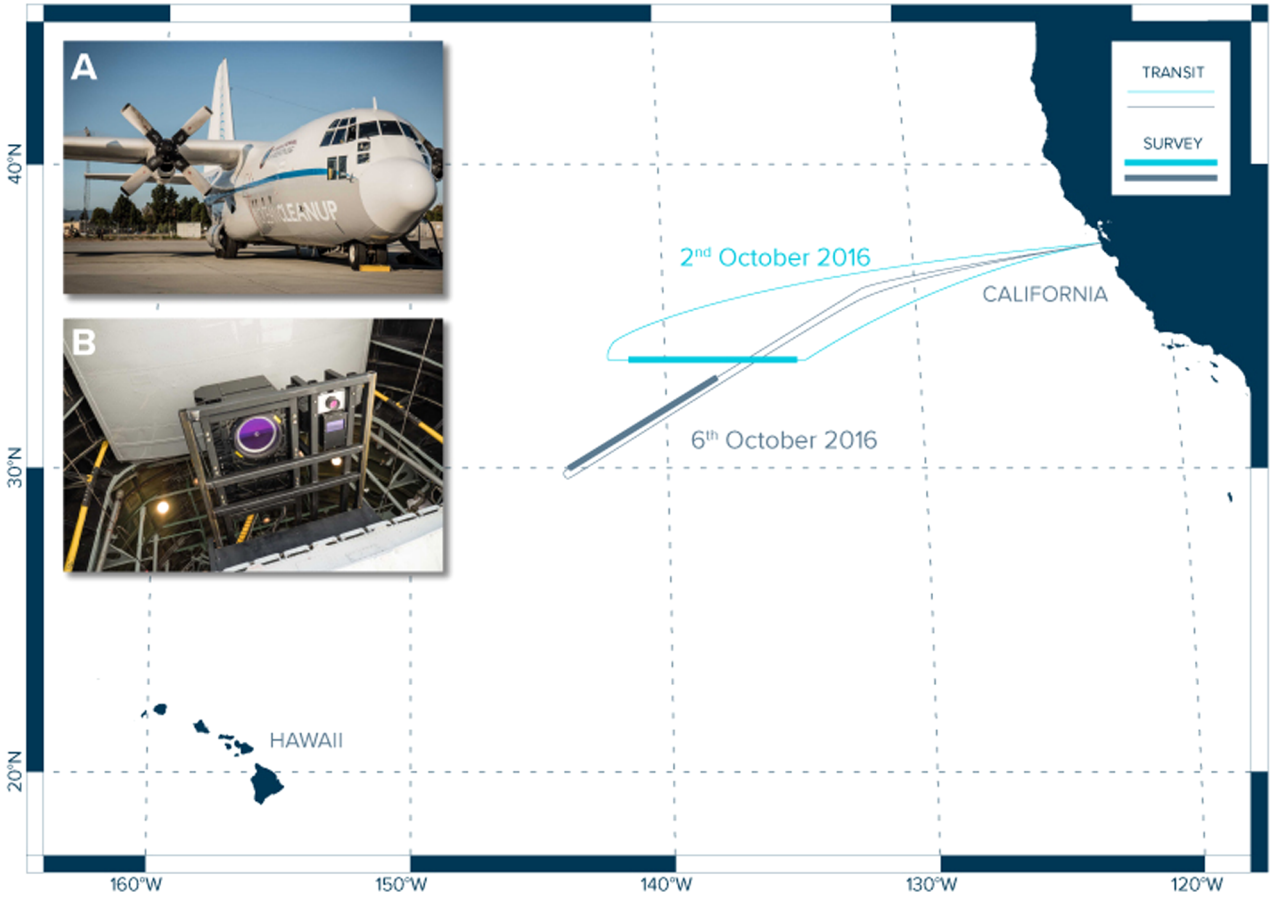

Figure 1. Map showing the area surveyed on October 2 (light blue track) and October 6 (dark blue track) 2016. While in survey mode (thicker lines), the sea surface area below the aircraft was imaged with a SWIR imager and a RGB camera. (A) Image of the Lockheed C-130 Hercules aircraft used in this study. (B) Customized frame used to attach the SASI imager and the RGB camera to the rear ramp of the aircraft, at nadir position. We also surveyed the area with a bathymetric lidar, but the results are not described in this study.

qualitative information on a wide geographical scale. Being able to remotely sense ocean plastics would allow us to build the much-needed knowledge base for understanding the amount and behavior of ocean plastics. Nonetheless, to date, only a handful of ocean plastic investigations have explored potential applications of satellite and airborne remote sensing tools for assessing ocean plastic pollution.[15,16]

Imaging optical sensors may allow for automated, non-invasive, and unmanned detection of marine litter, generating measurements that can assist in better estimating their concentrations and composition. Airborne hyperspectral imagers are capable of generating crucial complementary benchmark data on ocean plastic pollution due to their high spectral and geospatial resolution. At present, airborne platforms seem to be a promising source of evidence-based information for the calibration and validation of future satellite missions with the capabilities of detecting, tracking, identifying, and/or quantifying ocean plastics.[17,18] They can be considered a technological intermediary between satellite and near surface remote sensing. In a land-based investigation, hyperspectral imaging and detection algorithm development were completed over known targets including natural and synthetic hydrocarbons.[19,20] More recently, optical properties of both micro- (<5 mm) and macro- (>5 mm) marine-harvested plastics have been investigated along with a case study showing the potential of remote detection and polymer identification of wet and dry plastics on land.[18] Techniques have also been proposed for measuring and understanding spectral reflectance of floating marine macroplastics.[21] In June 2018, floating artificial targets of common ocean plastics were successfully detected from drones and satellite missions (e.g., PlanetScope Dove, Sentinel, TanDEM-X, WorldView) as part of the "Plastic Litter Project 2018: Drone Mapping and Satellite Testing for Marine Plastic on Aegean Sea" led by a team of researchers at the University of Aegean, Greece.

Here, we highlight the potential of a hyperspectral imager shortwave infrared (SWIR) imager to remotely detect ocean plastics. We did so by exploring spectra of floating ocean plastic pieces collected by a shortwave airborne spectrographic imager 600 (SASI) at an altitude of 400 m over an oceanic plastic pollution hotspot known as the North Pacific Accumulation Zone or the “Great Pacific Garbage Patch” (GPGP). We first identified ocean plastics in the true-color red, green, and blue (RGB) camera mosaics and then geolocated them in the SWIR imagery to extract their SWIR spectra. We also evaluated applications of SWIR imagers to the field of ocean plastic remote sensing. To the best of our knowledge, this study presents the first results of airborne SWIR remote sensing of ocean plastics, thus providing groundwork for future monitoring of plastics across oceans and other aquatic environments.

DOI: 10.1021/acs.est.8b02855
Environ. Sci. Technol. 2018, 52, 11699−11707

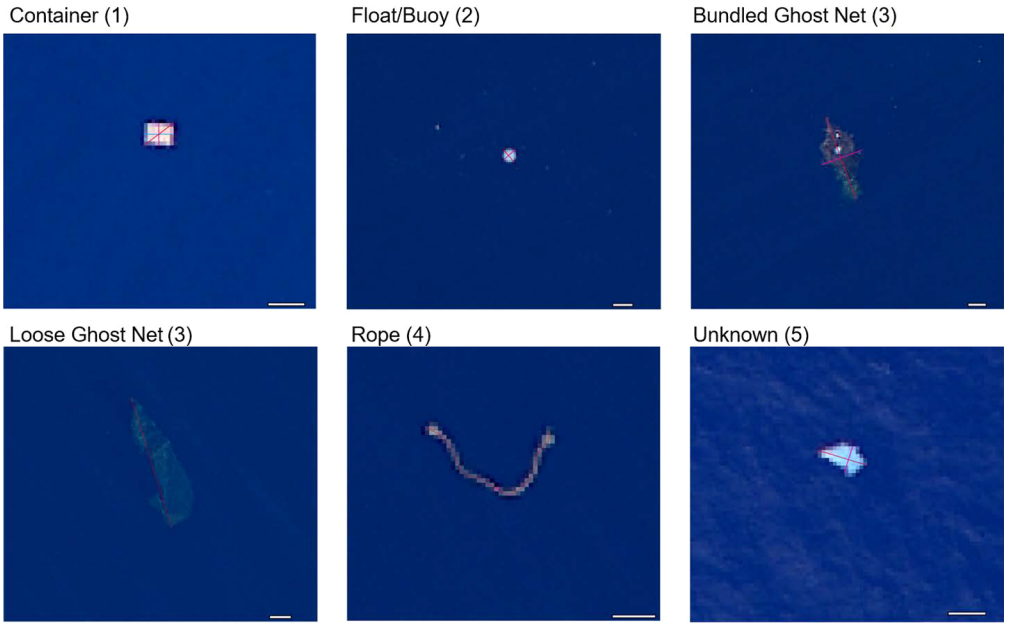

Figure 2. Examples of ocean plastic types (1−5) observed in the RGB imagery showing variability in piece size, shape, and color. Two kinds of ghost nets observed were bundled nets and loose nets. Lines above objects show some of the measurements taken. Scale = 1 m. Image modified after ref 6.

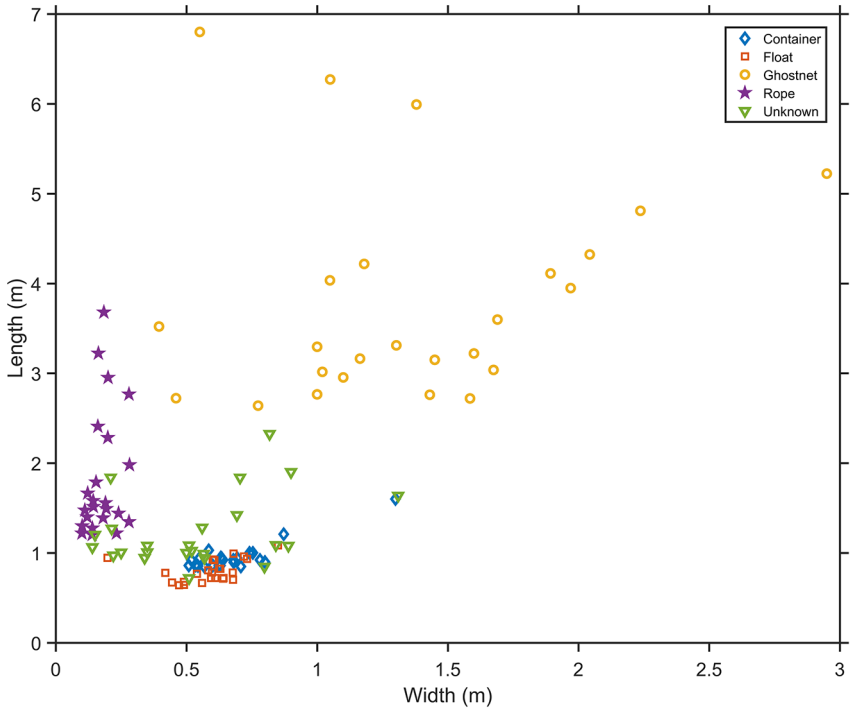

Figure 3. Length and width of the ocean plastic objects used in this study (N = 118).

MATERIALS AND METHODS

Field Campaign. Aerial surveys were conducted over the GPGP onboard a manned International Air Response Lockheed C-130 Hercules aircraft on October 2 and 6, 2016 (Figure 1). After a 5 h transit from San Francisco to the GPGP area, the aircraft dropped to 400 m above sea level and set the ground speed to 140 knots. Both surveys lasted for approximately 2.5 h, with the first (October 2) and second (October 6) flights having trajectory lengths equal to 668 and 686 km, respectively. Hyperspectral imagery was captured using a high-performance state-of-the-art ITRES SASI-600 push broom line scanning imager with 100 wavebands in the SWIR region, ranging from 950 to 2450 nm, at 15 nm spectral resolution. Sea surface RGB images were simultaneously captured by a high spatial resolution Optech CS-4800i 16 megapixel frame camera, at one frame per second intervals. The spatial resolution of the SASI imager was 0.5 m across × 1.2 m along the track resolution and 0.1 m × 0.1 m for the RGB camera. The solar elevation angle during the first flight varied between 38° (1156 local start time) and 52° (1410 local

DOI: 10.1021/acs.est.8b02855
Environ. Sci. Technol. 2018, 52, 11699−11707

end time), with solar azimuth angles of 130° and 188° at the start and end times, respectively. For the second flight, the solar elevation was 52° at the start of the survey (1514 local time) and 28.5° at the end (1721 local time), with solar azimuth angles equal to 201° at the start time (1514 local time) and 240° at the end time (1721 local time). The sea state was calm during both flights, with whitecaps in certain periods of the surveys. The sky was clear with a few high cirrus and high stratus during the whole first flight and most periods of the second flight. The latter also had some sporadic periods with low clouds and fog just above the sea surface that disrupted our survey.

Selection of Debris for Analyses. This study explores information from a fraction (N = 118 items) of the ocean plastics found in the RGB mosaics (N = 1595 items). Details on RGB image processing and ocean plastic characterization (e.g., object size distribution) are available in ref 6. In brief, the RGB images were georeferenced using integrated global navigation satellite/inertial measurement unit systems and converted into single-frame mosaics. The ocean plastic identification was done by trained observers and complemented by a custom-made automated detection algorithm. Metadata of each ocean plastic piece identified included its latitude, longitude, length, width, color, and object type: (1) "container" − rectangular bright objects such as fishing crates and drums; (2) "float" − rounded bright objects; (3) "ghost nets" − either a colorful group of various fishing nets bundled together or a single translucent fishing net; (4) "rope" − long cylindrical objects around 0.15 m thick; and (5) "unknown" − objects that are clearly debris but whose object type could not be identified (Figure 2).

For this study, we selected the top 30 largest items (in length) within each of the ocean plastic type categories (N = 150 selected items). By using the QGIS Las Palmas 2.18 LTR software, SWIR images were overlaid on top of the RGB images containing the selected items. To better visualize the overlaying image, the SWIR image transparency was adjusted thus allowing identification of pixel borders after zooming into target objects. As the RGB and SASI imagery collections were not always synchronous, we were unable to locate a few items in the SWIR imagery and ended up with 118 out of the 150 selected debris: 24 containers, 23 floats, 25 ghost nets, 23 ropes, and 23 unknown items. The average debris length and width (±standard deviation) were equal to 1.62 ± 1.20 m and 0.63 ± 0.44 m, respectively (Figure 3). These pieces had a variety of colors, such as white, yellow, brown, blue, and other multicolored pieces composed of bundled nets of different types. Shape-wise, the pieces ranged from regular to irregular shapes, which could be the result of fragmentation by different processes at sea, including weathering, breaking waves, and photodegradation. Other relevant but unknown object properties that are likely to affect spectral signals include transparency level, surface texture (specular or diffuse spectral properties), and three-dimensional shape.

SWIR At-Sensor Radiance of Ocean Plastics. SWIR imagery analyses were performed in Harris Geospatial Solutions ENVI Classic 5.0 and QGIS software. For each of the 118 pieces located in the SWIR imagery, we retrieved spectral data from at least 2 pixels. No atmospheric correction was applied to the imagery to mitigate errors that could arise from any correction scheme implemented. This decision was also based on the lack of concurrent quantitative measurements to fully parametrize the atmosphere and sea-truth spectral information for intercomparison and validation tasks. Moreover, our analysis focused on narrow band spectral features specific to plastics that should be minimally impacted from atmospheric absorption. Further spectral data and statistical analyses were completed using MathWorks MATLAB R2015b. The Spearman rank correlation coefficient (ρ) was used to indicate the degree of association between spectra at a statistical significance threshold of $p < 0.01$. The differences in magnitude were derived using the unbiased percentage difference (UPD) between spectra.[22] The signal shape similarities between spectra were quantified using the spectral contrast angle with eq 1:

$$\theta = \cos^{-1} \frac{\sum x \cdot y}{\sqrt{\sum x^2 \sum y^2}} \quad (1)$$

where x and y are different spectra. A θ value equal to 0° suggests a very strong spectral shape similarity, and θ = 90° suggests very weak spectral shape identity. The goodness of spectral shape similarity was defined as very strong ($0° \le \theta \le 5°$), strong ($5° < \theta \le 10°$), moderate ($10° < \theta \le 15°$), weak ($15° < \theta \le 20°$), and very weak ($20° < \theta$), as proposed by ref 18.

Detailed Analyses of a Ghost Net. We did a series of analyses using information from a large ghost net (Figure 4)

Figure 4. RGB image of the ghost net used for most of the analyses described in this study. Red stars show regions where spectral information from the SWIR imagery were extracted: "floating part" (star 1), "submerged part" (star 2), and "seawater" (stars 3−6).

where spectral information from 11 SWIR pixels could be retrieved. This was the most appropriate object of this study that covered a full SWIR pixel (i.e., with no seawater regions within the pixel). By visually inspecting the finer resolution RGB image pixel by pixel, we classified the different parts of the ghost net into an area that is likely above seawater (called "floating part" thereafter), another that seems to be partially or entirely underwater (called "submerged part" thereafter), and seawater regions surrounding the object. We then explored the effect of seawater in the SWIR radiance (magnitude and shape) by extracting spectral information from pixels at these different ghost net areas. Absorption features in the spectra of the floating and submerged parts were identified using first derivative algorithms and a scale-space peak seeking algorithm.[23] The robust peak seeking algorithm used here iteratively smooths noisy data while increasing the length scales and then identifies peaks as the remaining maxima based on a scoring system.[23]

We also assessed the possibility of distinguishing the polymer type of the selected ghost net by matching the at-

DOI: 10.1021/acs.est.8b02855
Environ. Sci. Technol. 2018, 52, 11699−11707

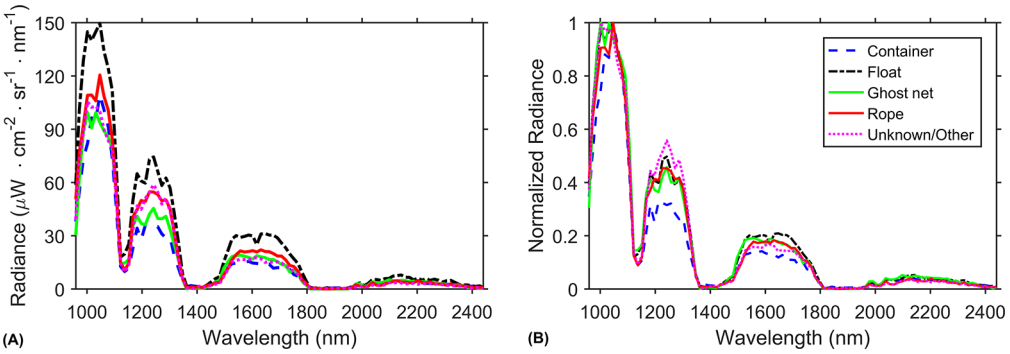

Figure 5. Spectral at-sensor radiance (950−2450 nm) of ocean plastics (N = 118 items) from the GPGP: (A) Median and (B) median normalized to the maximum spectral at-sensor radiance of different ocean plastic types.

sensor radiance spectra against spectra from an open access library containing spectral reflectance information extracted from virgin pellets of the following polymer types: polyvinyl chloride (PVC), polyamide or nylon (PA 6.6 and PA 6), low-density polyethylene (LDPE), polyethylene terephthalate (PET), polypropylene (PP), polystyrene (PS), fluorinated ethylene propylene Teflon (FEP), terpolymer Lustran 752 (ABS), Merlon, and poly(methyl methacrylate) (PMMA).[24] Spectral resampling of the reference library data set (1 nm spectral resolution) was performed to match our SASI imagery (15 nm spectral resolution) by averaging the reference library spectra over each SASI waveband. For the purpose of this proof-of-concept study, we assumed the normalized to maximum at-sensor radiance spectral shape is nearly identical to the at-sensor reflectance.

Finally, we applied spectral unmixing to the ghost net spectra information to simulate how ocean plastics can be quantified per pixel coverage. Spectral unmixing is a classic approach useful in estimating pixel coverage of known materials based on the bulk spectral properties of known endmembers in a target pixel. The approach assumes that, in a target pixel, there are various disparate optically active components that contribute uniquely to the bulk spectral signal reaching a sensor.[25−27] Therefore, the fractions of the spectral signal contributed by each optically active component within a pixel can be transformed into numerical fractional abundance descriptors, such as percentage coverage per pixel. Typically, a simple linear or sophisticated nonlinear model is applied to decompose the bulk spectral signal from a pixel. Here, we utilized a simple linear model that assumed seawater and floating ocean plastics as the major contributors or endmembers to the bulk reflected light reaching the SWIR imager. The water endmember was the averaged spectra of pixels surrounding the ghost net, and the ocean plastic endmember was the pixel above the floating part of the ghost net. We trust this ghost net pixel is our best representative of a 100% plastic pixel coverage due to its position (~100% on top of a floating plastic object) and its relatively high at-sensor radiance. We therefore use the at-sensor radiance (L) as a proxy of the inherent reflectance of the target, so the mixed L_{mix} was approximated with eq 2:

$$L_{mix} = f_{debris} \times L_{debris} + f_{seawater} \times L_{seawater} \quad (2)$$

where f is the proportion of each endmember ranging from 0 to 1 to the resulting simulated pixel L_{mix}. The absorption features were quantified using a continuum removed band depth algorithm.[28] For brevity, we use the following floating debris pixel: 5%, 25%, 50%, 75%, and 100%. We applied and assessed the applicability of the synthetic hydrocarbon indexes that have been used successfully to map land-based plastics at ~1215 nm (SASI waveband 1212.5 nm) and at ~1732 nm (SASI waveband 1737.5 nm) through an intervening atmosphere from an airborne imager.[18,20]

RESULTS AND DISCUSSION

SWIR At-Sensor Radiance of Ocean Plastics. The SWIR signal of the ocean plastics investigated in this study (N = 118) showed some variability in magnitude (Figure 5A) and shape (Figure 5B). These variabilities were quite consistent among ocean plastic types, with the median reflectance spectra of the different ocean plastic types being strongly correlated $\rho > 0.98$ and the spectral shape similarity indexes $\theta < 11°$. The later suggests the shapes of the median spectra of the different ocean plastic types were similar, with moderate similarities between the "unknown" and "container" types ($\theta = 10.7°$) and very strong similarities between ghost nets and floats ($\theta = 4.3°$). Spectral shape is an important metric in polymer identification utilizing spectral reference libraries, an approach recently evaluated in a study matching marine-harvested plastics to a spectral reference library of known virgin pellets.[18] In a similar way, methods such as Raman and Fourier transform IR spectroscopies determine the spectral signal of a sample, and then, identification is completed by best-matching the shape of the measured signal using statistical scoring methods to a known material signal in a spectral reference library. The similarities in spectral shapes found here could be a consequence of the relatively uniform polymer composition of GPGP plastics, as previous studies suggest they are mostly made of polyethylene (PE) and PP.[6]

Overall, floats had the highest radiance, possibly due to their high reflectivity and high buoyancy that could lead to little or no water above them meaning less light absorption by water. Containers had the lowest radiance, likely due to their relatively low buoyancy that leads to slightly more coverage by seawater. High (>62%) UPDs were noted around the 970, 1200, 1530, 1680, and 2100 nm wavebands. These absorption features coincide with some of those unique to plastics and are less likely to be affected by spectral properties of atmospheric gases.[18] The lowest UPDs between maximum and minimum at-sensor radiance (≈ 0%) were located around 1400 and 1900 nm, corresponding to wavelengths with strong absorption of light by atmospheric gases.

Influence of Seawater on Ocean Plastic SWIR Spectra. The spectral at-sensor radiance of the seawater pixels

DOI: 10.1021/acs.est.8b02855
Environ. Sci. Technol. 2018, 52, 11699−11707

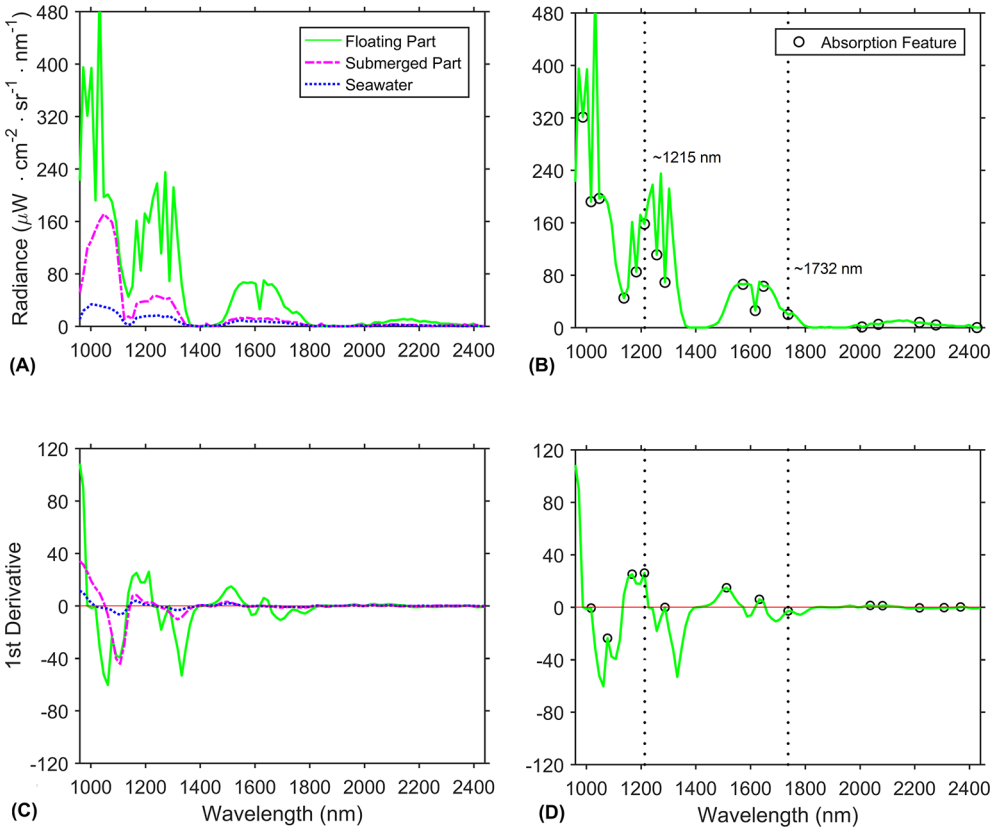

Figure 6. (A) Median spectra of floating and submerged parts of a ghost net and its surrounding seawater (see Figure 4). (B) Spectrum of the ghost net floating part and absorption features identified with a peak-seeking algorithm (black circles). Dotted lines highlight the absorption features around 1215 and 1732 nm used in our spectral unmixing simulations. (C) First derivative of the spectra shown in panel A. (D) Absorption features (black circles) identified in the first-derivative spectrum of the ghost net floating part.

Table 1. Spectral Contrast Angles (θ) and Spearman Rank Correlation Coefficients (ρ) Derived by Matching Spectral Properties of Floating and Submerged Parts of a Ghost Net[a]) to Spectra from a Reference Library[24] Containing Several Polymers[b]

	PVC	PA 6.6	PA 6	LDPE	PET	PP	PS	FEP	ABS	Merlon	PMMA
Floating											
θ	36	26	26	33	28	32	28	38	27	29	30
ρ	0.69	0.76	0.75	0.53	0.83	0.60	0.80	0.35	0.77	0.83	0.79
Submerged											
θ	45	31	31	38	37	37	34	47	34	37	38
ρ	0.76	0.82	0.82	0.61	0.89	0.69	0.83	0.20	0.81	0.87	0.86

[a] Figures 4 and 6. [b] Polyvinyl chloride (PVC), polyamide or nylon (PA 6.6 and PA 6), low-density polyethylene (LDPE), polyethylene terephthalate (PET), polypropylene (PP), polystyrene (PS), fluorinated ethylene propylene Teflon (FEP), terpolymer Lustran 752 (ABS), Merlon, and poly(methyl methacrylate) (PMMA).

surrounding a ghost net (see Figure 4) was lower than the ghost net pixels. Furthermore, ghost net pixels classified as "submerged" (see star 2 in Figure 4) exhibited lower radiance than the floating portion (see star 1 in Figure 4). Spectral absorption features were determined in the observed at-sensor radiance and the first-derivative spectra of both floating and submerged parts of the ghost net (Figure 6). The locations of these absorption features in both the observed at-sensor radiance and the first-derivative spectra were nearly identical (see Figure 6B, D). Several absorption features were identified in this plastic object but not in the seawater signal, for example, 1015, 1150, 1215, 1288, 1625, and 1732 nm. Of interest were the common absorption features around 1215 and 1732 nm found in both the submerged and floating parts, as well as prior studies.[18,20,29,30] Nonetheless, some absorption features were not all entirely the same in the ghost net parts that were above and below the sea surface. This is evidence that water and an intervening atmosphere above ocean plastics may influence both the magnitude and shape of the at-sensor radiance. Further studies where the level of debris submersion is known are needed to assess up to what depth the distinct spectral signal of marine plastics is detectable from both airborne and satellite platforms.

Polymer Identification. The absorption features identified in the ghost net floating part (see black circles in Figure 6) are common in plastics and other hydrocarbons.[18,29−32] Nonetheless, both the submerged and floating parts of this object had weak similarities with plastics from our spectral reference library, as evidenced by our spectral similarity scale θ varying from 26° to 47°, with positive statistically significant ρ ranging

DOI: 10.1021/acs.est.8b02855
Environ. Sci. Technol. 2018, 52, 11699−11707

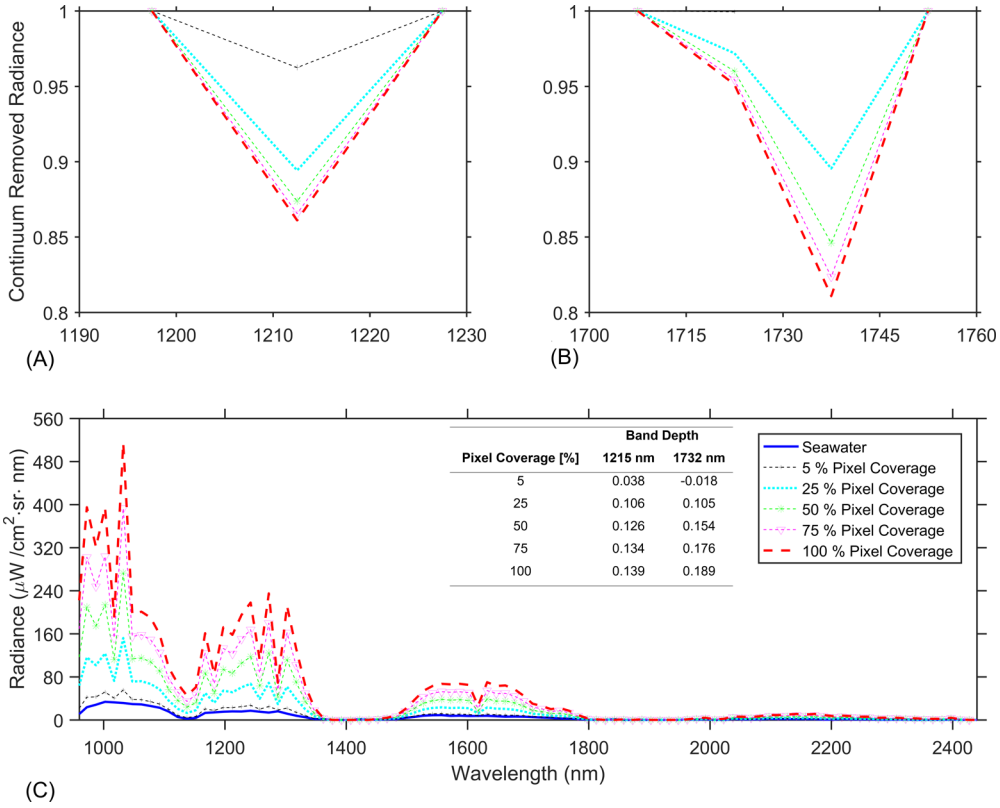

Figure 7. Spectral unmixing simulation using the floating part of the ghost net and seawater endmembers (see Figure 4). Continuum removed radiance at the (A) 1215 nm and (B) 1732 nm absorption features and (C) the at-sensor radiance over the measured spectrum range with changing pixel coverage by ocean plastics.

from 0.20 to 0.89 (Table 1). Taking the lowest θ values, the ghost net could consist of PA, PET, PS, PMMA, or PP. If we take polymer buoyancy into account, we could assume this net is likely made of PP, which is the only polymer among these that can float in seawater (due to its density being lower than that of seawater). This result corroborates with findings from previous studies concluding that PP fishing nets are very common within the GPGP area.[6] We believe our limited polymer matches were mostly due to seawater and atmosphere effects as well as unique ocean plastic characteristics resulting from natural weathering processes, photodegradation, and formation of biofilms. We suggest future studies to expand our spectral reference library by analyzing marine-harvested plastics from a wide range of locations, sizes, types, and levels of degradation. Ocean plastic size plays an important role on the resulting optical properties of polymers. As plastics breakdown, their physical and chemical properties might change in terms of composition, surface type (smooth for specular reflectance or rough for diffuse reflectance), shape (e.g., round or flat and solid or hollow), and transparency.[21,33] There is also a need to include more polymers in such a spectral reference library, particularly high-density polyethylene (HDPE) and expanded polystyrene (EPS), which are dominant types in sea surface environments.[6,13,34] Matching samples to such an expanded library would likely improve SWIR-based polymer identifications.

Potential for Ocean Plastic Pollution Quantification. The results from our spectral unmixing simulations agree well with prior results suggesting that the ∼1215 nm and ∼1732 nm features have potential for use in estimating ocean plastic pollution levels using information from SWIR sensors (Figure 7). Even though our study identified a few other absorption features that may also be useful for quantifying ocean plastic pollution (see Figures 5 and 6), our focus in this study was on using already known plastic absorption features[18,20,29,30] to further evaluate their use in ocean plastic research. The derived continuum band depth indexes at ∼1215 nm and ∼1732 nm suggest that, at 5% pixel coverage, the 1732 nm feature might not be appropriate for detecting ocean plastics. Future investigations matching in situ ocean plastic counts with pixel coverage information would be useful for validating algorithms capable of deriving plastic abundance (e.g., counts per unit area) from SWIR imagery. A decrease in the pixel coverage (related to contribution of the floating piece signal to the bulk signal reaching sensor L_{mix}) results in a decrease in the band depth at each absorption feature (Figure 7), a relationship consistent with literature.[25,26] The size distribution of observed pieces should be further investigated in relation to the pixel size (0.5 m × 1.2 m). We performed simple linear mixing and continuum removed band depth as a detection proxy for the presence of plastics. Theoretically, with the SASI instrument flying at an altitude of 400 m, there is potential in detecting a particle 0.025 m × 0.06 m in size, equivalent to the simulated 5% pixel coverage. This approximately falls in the mesoplastic (0.005−0.05 m) size class reported in a recent study.[6] More analyses to investigate the use of SWIR imaging for sensing ocean plastic are required to better account for variables such as the sensor signal-to-noise ratio, object depth, polymer type, debris size, edge effect in image classification, sea state, solar position, and meteorological conditions. Results of such studies would contribute toward manned and unmanned airborne as well as satellite remote sensing of ocean micro- and

DOI: 10.1021/acs.est.8b02855
Environ. Sci. Technol. 2018, 52, 11699−11707

macroplastic size groups, in terms of instrument design and algorithm development.

Monitoring of Ocean Plastics with Airborne Imagers. This study uses typical analysis approaches to demonstrate how the spectral at-sensor properties derived from SASI SWIR imagery can be used to distinguish ocean plastics from surrounding seawater using the unique absorption features of polymers. To improve our degree of certainty in distinguishing plastic spectrally, investigations into the effect of decreased radiance due to submersion or types of plastic are needed. It is also important to highlight that ocean plastic pollution research is a broad and interdisciplinary field, with spectral and spatial coverage requirements varying with the scientific question posed, the size of the particles of interest, and the following overarching goals: (i) detect, (ii) track, (iii) quantify, and (iv) identify ocean plastics.

We believe a simplified quantification and detection algorithm based on a band depth method requiring a minimum of three wavebands (one at the left and one at the right of the crest of the absorption feature as well as the absorption waveband itself) can be used for both features at ∼1215 and ∼1732 nm. A band difference or band ratio algorithm would only need two wavebands, something to be explored in the future. However, because of the diversity in ocean plastics, more wavebands and materials in the spectral reference library will be a prerequisite for better polymer identification. Furthermore, many hyperspectral imagers, such as the airborne visible IR imaging spectrometer (AVIRIS, 224 wavebands, 400−2500 nm) from the National Aeronautics and Space Administration and the airborne PRISM experiment spectrometer (APEX, 300 wavebands, 400−2500 nm) from the European Space Agency coupled with coincident RGB imagery, meteorological, and auxiliary sea-truth information for algorithm validation and calibration have potential applications in remote sensing of ocean plastics. Already, images captured over land by AVIRIS have been shown to be useful in mapping dry synthetic hydrocarbons.[18]

AUTHOR INFORMATION

Corresponding Author

*E-mail: shungu.garaba@uni-oldenburg.de.

ORCID

Shungudzemwoyo P. Garaba: 0000-0002-9656-3881

Julia Reisser: 0000-0002-1785-1042

Notes

The authors declare no competing financial interest.

ACKNOWLEDGMENTS

We would like to thank donors of The Ocean Cleanup and partners of the "Aerial Expedition" project. Partners included International Air Response, ITRES, Teledyne Optech, Salesforce and Google for Moffett Airfield sponsorship. We also thank NOARC for the collaboration and support with acquiring the SWIR data over the North Pacific. We are grateful for assistance on the project by Robert Marthouse. We acknowledge Rick Martini and Anna Schwarz for support with logistics and survey planning; Chandra Salgado, Sue Gibbs, Kim Noble, Sara Niksic, Florent Beauverd, and Taylor Swift for assistance with the field work; and Sara Hajbane and Igor Carneiro for postprocessing of the RGB mosaics. We appreciate the fellowship funded by NASA Ocean Biology and Biogeochemistry Grant No. NNX15AC32G.

REFERENCES

(1) G20. Annex to G20 Leaders Declaration: G20 Action Plan on Marine Litter. In *G20 Summit 2017*; Federal Ministry for the Environment, Nature Conservation, Building and Nuclear Safety: Hamburg, Germany, 2017; p 7.

(2) Werner, S.; Budziak, A.; van Franeker, J.; Galgani, F.; Hanke, G.; Maes, T.; Matiddi, M.; Nilsson, P.; Oosterbaan, L.; Priestland, E.; Thompson, R.; Veiga, J.; Vlachogianni, T. *Harm Caused by Marine Litter*; Publications Office of the European Union: Luxembourg, 2016; p 92.

(3) Bergmann, M.; Wirzberger, V.; Krumpen, T.; Lorenz, C.; Primpke, S.; Tekman, M. B.; Gerdts, G. High Quantities of Microplastic in Arctic Deep-Sea Sediments from the HAUSGARTEN Observatory. *Environ. Sci. Technol.* **2017**, *51* (19), 11000−11010.

(4) Maximenko, N.; Hafner, J.; Niiler, P. Pathways of marine debris derived from trajectories of Lagrangian drifters. *Mar. Pollut. Bull.* **2012**, *65* (1−3), 51−62.

(5) van Sebille, E.; Wilcox, C.; Lebreton, L.; Maximenko, N.; Hardesty, B. D.; van Franeker, J. A.; Eriksen, M.; Siegel, D.; Galgani, F.; Law, K. L. A global inventory of small floating plastic debris. *Environ. Res. Lett.* **2015**, *10* (12), 124006.

(6) Lebreton, L.; Slat, B.; Ferrari, F.; Sainte-Rose, B.; Aitken, J.; Marthouse, R.; Hajbane, S.; Cunsolo, S.; Schwarz, A.; Levivier, A.; Noble, K.; Debeljak, P.; Maral, H.; Schoeneich-Argent, R.; Brambini, R.; Reisser, J. Evidence that the Great Pacific Garbage Patch is rapidly accumulating plastic. *Sci. Rep.* **2018**, *8* (1), 4666.

(7) Cózar, A.; Echevarría, F.; González-Gordillo, J. I.; Irigoien, X.; Úbeda, B.; Hernández-León, S.; Palma, Á. T.; Navarro, S.; García-de-Lomas, J.; Ruiz, A.; Fernández-de-Puelles, M. L.; Duarte, C. M. Plastic debris in the open ocean. *Proc. Natl. Acad. Sci. U. S. A.* **2014**, *111* (28), 10239−10244.

(8) Law, K. L.; Morét-Ferguson, S. E.; Goodwin, D. S.; Zettler, E. R.; DeForce, E.; Kukulka, T.; Proskurowski, G. Distribution of Surface Plastic Debris in the Eastern Pacific Ocean from an 11-Year Data Set. *Environ. Sci. Technol.* **2014**, *48* (9), 4732−4738.

(9) Reisser, J.; Shaw, J.; Wilcox, C.; Hardesty, B. D.; Proietti, M.; Thums, M.; Pattiaratchi, C. Marine plastic pollution in waters around Australia: Characteristics, concentrations, and pathways. *PLoS One* **2013**, *8* (11), e80466.

(10) Carpenter, E. J.; Smith, K. L. Plastics on the Sargasso Sea Surface. *Science* **1972**, *175* (4027), 1240−1241.

(11) Jambeck, J. R.; Geyer, R.; Wilcox, C.; Siegler, T. R.; Perryman, M.; Andrady, A.; Narayan, R.; Law, K. L. Plastic waste inputs from land into the ocean. *Science* **2015**, *347* (6223), 768−771.

(12) Lebreton, L. C. M.; van der Zwet, J.; Damsteeg, J.-W.; Slat, B.; Andrady, A.; Reisser, J. River plastic emissions to the world's oceans. *Nat. Commun.* **2017**, *8*, 15611.

(13) Eriksen, M.; Lebreton, L. C. M.; Carson, H. S.; Thiel, M.; Moore, C. J.; Borerro, J. C.; Galgani, F.; Ryan, P. G.; Reisser, J. Plastic Pollution in the World's Oceans: More than 5 Trillion Plastic Pieces Weighing over 250,000 Tons Afloat at Sea. *PLoS One* **2014**, *9* (12), e111913.

(14) Kooi, M.; Reisser, J.; Slat, B.; Ferrari, F. F.; Schmid, M. S.; Cunsolo, S.; Brambini, R.; Noble, K.; Sirks, L.-A.; Linders, T. E. W.; Schoeneich-Argent, R. I.; Koelmans, A. A. The effect of particle properties on the depth profile of buoyant plastics in the ocean. *Sci. Rep.* **2016**, *6*, 33882.

(15) Pichel, W. G.; Veenstra, T. S.; Churnside, J. H.; Arabini, E.; Friedman, K. S.; Foley, D. G.; Brainard, R. E.; Kiefer, D.; Ogle, S.; Clemente-Colón, P.; Li, X. GhostNet marine debris survey in the Gulf of Alaska − Satellite guidance and aircraft observations. *Mar. Pollut. Bull.* **2012**, *65* (1−3), 28−41.

(16) Aoyama, T. Extraction of marine debris in the Sea of Japan using high-spatial-resolution satellite images. In *Remote Sensing of the Oceans and Inland Waters: Techniques, Applications, and Challenges*; Frouin, R. J., Shenoi, S. C., Rao, K. H., Eds.; Proceedings of SPIE Vol. 9878; SPIE: Bellingham, WA, 2016; p 987817.

DOI: 10.1021/acs.est.8b02855
Environ. Sci. Technol. 2018, 52, 11699−11707

(17) Mace, T. H. At-sea detection of marine debris: Overview of technologies, processes, issues, and options. *Mar. Pollut. Bull.* **2012**, *65* (1−3), 23−27.
(18) Garaba, S. P.; Dierssen, H. M. An airborne remote sensing case study of synthetic hydrocarbon detection using short wave infrared absorption features identified from marine-harvested macro- and microplastics. *Remote Sens. Environ.* **2018**, *205*, 224−235.
(19) Hörig, B.; Kühn, F.; Oschütz, F.; Lehmann, F. HyMap hyperspectral remote sensing to detect hydrocarbons. *Int. J. Remote Sens.* **2001**, *22* (8), 1413−1422.
(20) Kühn, F.; Oppermann, K.; Hörig, B. Hydrocarbon Index − an algorithm for hyperspectral detection of hydrocarbons. *Int. J. Remote Sens.* **2004**, *25* (12), 2467−2473.
(21) Goddijn-Murphy, L.; Peters, S.; van Sebille, E.; James, N. A.; Gibb, S. Concept for a hyperspectral remote sensing algorithm for floating marine macro plastics. *Mar. Pollut. Bull.* **2018**, *126*, 255−262.
(22) Hooker, S. B.; Lazin, G.; Zibordi, G.; McLean, S. An evaluation of above- and in-water methods for determining water-leaving radiances. *J. Atmos. Ocean. Technol.* **2002**, *19* (4), 486−515.
(23) Liutkus, A. *Scale-space peak picking: Inria, Speech Processing Team*; Inria Nancy - Grand Est: Villers-lès-Nancy, France, 2015.
(24) Garaba, S. P.; Dierssen, H. M. Spectral reference library of 11 types of virgin plastic pellets common in marine plastic debris. Data set [Online]; http://ecosis.org from the Ecological Spectral Information System (EcoSIS); DOI: 10.21232/C27H34.
(25) Settle, J. J.; Drake, N. A. Linear mixing and the estimation of ground cover proportions. *Int. J. Remote Sens.* **1993**, *14* (6), 1159−1177.
(26) Keshava, N.; Mustard, J. F. Spectral unmixing. *IEEE Signal Proc. Mag.* **2002**, *19* (1), 44−57.
(27) Adams, J. B.; Smith, M. O.; Johnson, P. E. Spectral mixture modeling: A new analysis of rock and soil types at the Viking Lander 1 Site. *J. Geophys. Res.* **1986**, *91* (B8), 8098−8112.
(28) Clark, R. N. Spectral properties of mixtures of montmorillonite and dark carbon grains: Implications for remote sensing minerals containing chemically and physically adsorbed water. *J. Geophys. Res. Solid Earth* **1983**, *88* (B12), 10635−10644.
(29) Cloutis, E. A. Spectral reflectance properties of hydrocarbons: Remote-sensing implications. *Science* **1989**, *245* (4914), 165−168.
(30) Asadzadeh, S.; de Souza Filho, C. R. Spectral remote sensing for onshore seepage characterization: A critical overview. *Earth-Sci. Rev.* **2017**, *168*, 48−72.
(31) Huth-Fehre, T.; Feldhoff, R.; Kantimm, T.; Quick, L.; Winter, F.; Cammann, K.; van den Broek, W.; Wienke, D.; Melssen, W.; Buydens, L. NIR - Remote sensing and artificial neural networks for rapid identification of post consumer plastics. *J. Mol. Struct.* **1995**, *348* (0), 143−146.
(32) Chung, H.; Choi, H. J.; Ku, M. S. Rapid identification of petroleum products by near-infrared spectroscopy. *Bull. Korean Chem. Soc.* **1999**, *20* (9), 1021−1025.
(33) Filella, M. Questions of size and numbers in environmental research on microplastics: methodological and conceptual aspects. *Environ. Chem.* **2015**, *12* (5), 527−538.
(34) Morét-Ferguson, S.; Law, K. L.; Proskurowski, G.; Murphy, E. K.; Peacock, E. E.; Reddy, C. M. The size, mass, and composition of plastic debris in the western North Atlantic Ocean. *Mar. Pollut. Bull.* **2010**, *60* (10), 1873−1878.

DOI: 10.1021/acs.est.8b02855
Environ. Sci. Technol. 2018, 52, 11699−11707